Exploratory Observations of Winter Oceanographic Conditions in the Saguenay Fjord

Daniel Bourgault[1,*], Peter S. Galbraith[2] and Gesche Winkler[1]

[1]*Institut des sciences de la mer de Rimouski, Rimouski, Quebec, Canada*
[2]*Department of Fisheries and Oceans Canada, Mont-Joli, Quebec, Canada*

[Original manuscript received 3 June 2011; accepted 31 October 2011]

ABSTRACT *A literature review and a search through public databases revealed that little attention had been paid to the winter oceanographic conditions of the Saguenay Fjord. This observation led to an exploratory survey carried out in the Saguenay Fjord during winter 2010, providing the first historical winter measurements throughout the entire water column. Contrary to hypotheses raised about 40 years earlier, the winter water column was well stratified both in temperature and salinity with a dynamically stable pycnocline. The water column was, in fact, more stratified than during the previous summer with a thinner and fresher surface layer lying above a sharper halocline. This stronger winter stratification is attributed to the shielding effect of sea ice to wind-induced mixing. An intermediate water mass lying between 20 and 60 m, called the Saguenay Intermediate Water (SIW), is identified and documented. This water mass appeared clearly as a warm intermediate layer during winter 2010. It is hypothesized that SIW was formed during the previous summer as a mixture of St. Lawrence Estuary Cold Intermediate Layer (CIL), found at flood tide near the mouth of the fjord, and surface water from the Saguenay Fjord. It is further hypothesized that during winter the SIW is eroded and mixed with cold and salty water from the St. Lawrence Estuary found near the mouth of the fjord. This new mixture creates the* T-S *characteristics of the Saguenay Deep Water (i.e., the water mass that fills the bottom of the Saguenay Fjord). A wintertime water-column echogram is also presented. The echogram reveals a series of biological strata with small fish near the top of the water column (5–20 m), showing little movement, and active larger fish at mid-depth (below 80 m). The echogram also shows vertical migration of zooplankton, possibly euphausiids, mysids or hyperiid amphipod occurring at sunset. Turbulence measured through the migration does not show evidence of enhanced turbulent diffusivity.*

RÉSUMÉ *[Traduit par la rédaction] L'analyse documentaire et la recherche dans des bases de données publiques que nous avons effectuées ont permis d'établir que peu d'études portent sur les conditions océanographiques en hiver dans le fjord du Saguenay. Voilà pourquoi nous avons procédé à une étude de reconnaissance dans le fjord pendant l'hiver 2010 afin de recueillir les premières mesures hivernales historiques dans l'ensemble de la colonne d'eau. Contrairement aux hypothèses avancées il y a une quarantaine d'années, la colonne d'eau en période hivernale était bien stratifiée du point de vue de la température et de la salinité et elle présentait une pycnocline stable sur le plan dynamique. En réalité, la colonne d'eau était plus stratifiée qu'au cours de la période estivale précédente : une mince couche d'eau douce en surface au contact d'une halocline prononcée. La stratification plus forte en hiver est attribuable à l'effet de protection de la glace marine par rapport au brassage induit par le vent. Nous avons établi l'existence d'une masse d'eau couche intermédiaire située à une profondeur variant de 20 à 60 m, appelée ici couche intermédiaire du Saguenay (SIW), et nous l'avons décrite. Pendant l'hiver 2010, cette masse d'eau apparaisait clairement comme une couche intermédiare chaude. Nous formons l'hypothèse que la SIW s'est formée l'été précédent, par le mélange de la couche intermédiaire froide (CIL) de l'estuaire du Saint-Laurent, observée à la marée montante à l'embouchure du fjord, et de la couche d'eau en surface du fjord du Saguenay. Nous postulons également que l'hiver, la SIW est érodée par mélange avec l'eau froide et salée de l'estuaire du Saint-Laurent qui se trouve à proximité de l'embouchure du Saguenay. Ce mélange confère sa température et salinité aux eaux profondes du Saguenay (c'est-à-dire la masse d'eau au fond du fjord du Saguenay). Nous présentons également un échogramme de la colonne d'eau en période hivernale. L'échogramme révèle une série de strates contenant de petits poissons dans le haut de la colonne d'eau (5 à 20 m), pratiquement immobiles, et de gros poissons actifs en zone intermédiaire (sous les 80 m). L'échogramme révèle également des migrations verticales de zooplancton à la brunante possiblement composées d'euphausiacés, de mysididés ou d'amphipodes hypéridés. Nous avons mesuré la turbulence pendant la migration, mais nous n'avons pas relevé d'indices d'augmentation de la diffusivité turbulente.*

[*]Corresponding author's email: daniel_bourgault@uqar.ca

ATMOSPHERE-OCEAN 50 (1) 2012, 17–30 http://dx.doi.org/10.1080/07055900.2012.659844
Canadian Meteorological and Oceanographic Society

1 Introduction

The variability of Arctic sea ice and predictions of its reduction (Stroeve et al., 2007; Comiso et al., 2008; Holland et al., 2008; Parkinson and Cavalieri, 2008) have been motivating factors, in the last decade, for large research programs on ice-covered marine ecosystems in the Canadian Arctic and related seas such as the Canadian Arctic Shelf Exchange Study (CASES; Fortier et al., 2008) and the Circumpolar Flaw Lead (CFL) program (Barber et al., 2010). In comparison, Canadian ice-covered marine ecosystems unconnected to the Arctic, such as the Gulf of St. Lawrence and eastern Canadian fjords, have received little research attention even though these subarctic systems are subject to comparable interannual and climatic sea-ice variabilities (Fig. 1). For example, over the most recent climate period (1981–2010), sea-ice coverage in the Gulf of St. Lawrence has decreased at a mean rate of 1.0% per year, compared to 1.5% per year for the Canadian Arctic, with a record low in the Gulf of St. Lawrence in 2010 with a 74% reduction relative to the 1969–2010 mean (Fig. 1).

Many questions motivating oceanographic research in the Canadian Arctic could be addressed by research in subarctic ice-covered environments. One such system is the Saguenay Fjord in eastern Canada (Fig. 2). This fjord shares some characteristics with coastal Arctic marine ecosystems; it is seasonally ice-covered; it receives important freshwater runoff; it is adjacent to a polynya (discussed below); it hosts many species of plankton, fish, marine mammals and birds; and it plays important economic and social roles for local communities (e.g., whale watching, boat tours, ice fishing). The Saguenay Fjord is also subject to important anthropogenic stresses (Pelletier and Sévigny, 2009). Furthermore, the fjord is part of the Saguenay–St. Lawrence Marine Park, the first national saltwater marine conservation area in Canada.

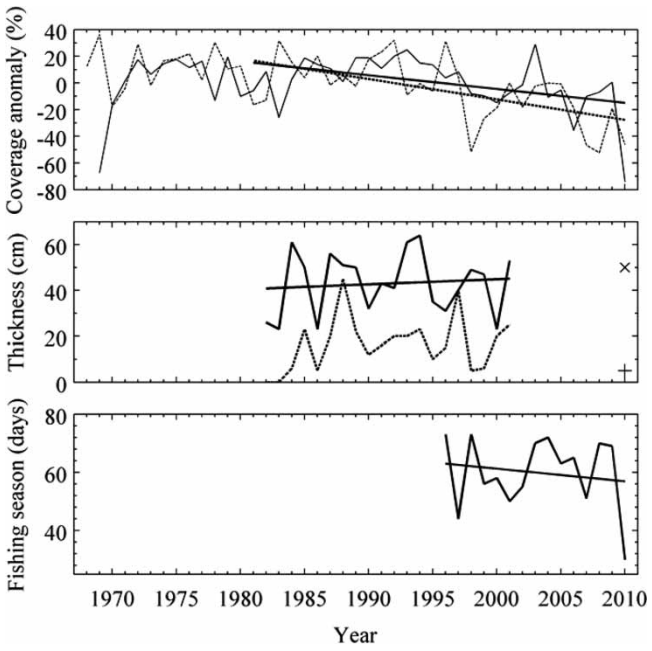

Fig. 1 (top panel) Sea-ice coverage anomaly in the Canadian Arctic (dashed line, relative to the 1969–2009 period) and Gulf of St. Lawrence (solid line, relative to the 1969–2010 period). These statistics are based on the minimum summer ice coverage for the Canadian Arctic and the maximum winter coverage for the Gulf of St. Lawrence. The straight lines are trends over the last 30 years. (middle panel) Maximum ice (solid line) and snow (dashed line) thickness measured near Anse Saint-Jean. (bottom panel) Duration of the ice fishing season. Data in the top and middle panels were retrieved online from EC (2011b). Data in the bottom panel are from DFO (2011a).

While summer oceanographic conditions in the fjord are well documented (Schafer et al., 1990; Pelletier and Sévigny, 2009), little is known about its winter conditions. In fact, there is not a single winter temperature-salinity profile available in the Oceanographic Data Management System database (DFO, 2011b) even though this unique marine park has been in existence for 10 years.

Motivated by the negative climatic trend of sea ice in subarctic eastern Canada, by the relevance of studying subarctic ice-covered marine ecosystems to address fundamental oceanographic questions related to boreal seas, by the limited winter observations available, and by the importance of Canadian subarctic waters for fisheries, tourism, shipping and oil and gas exploration, we carried out an exploratory survey in the ice-covered Saguenay Fjord. Our goals were to collect preliminary observations to characterize the basic oceanography of this fjord during the ice-covered season and to examine the feasibility of setting up ice camps for eventual longer-term seasonal studies. We provide here a review of the known characteristics of the winter conditions in the Saguenay Fjord (Section 2) and we report our observations (Section 4) against which some hypotheses raised more than 40 years ago by Drainville (1968) about the winter temperature-salinity structure are re-examined (Section 5).

2 The Saguenay Fjord

a *Geographical Context*

The Saguenay Fjord (Figs 2 and 3) is about 110 km long and 2 km wide, on average, and can be geomorphologically divided into Lower, Middle and Upper sections (Locat and Lévesque, 2009). The Lower Fjord, with a maximum depth of 260 m, has three major sills: the first of depth 20 m at the mouth, the second of depth 60 m at kilometre 18 and the third of depth 120 m at kilometre 32 (Fig. 3). These sills limit the exchange of deep water with the St. Lawrence Estuary (Bélanger, 2003) and are probable hot spots for tidal dissipation, turbulent mixing and internal wave generation (Stacey and Gratton, 2001; Janes, 2009; Bourgault et al., 2011). The Middle Fjord is approximately 45 km long and is characterized by a much flatter bathymetry than the Lower Fjord with a depth of approximately 250 m and without any prominent sills. The Upper Fjord is the shallowing portion between the deep Middle Fjord and the Saguenay River delta.

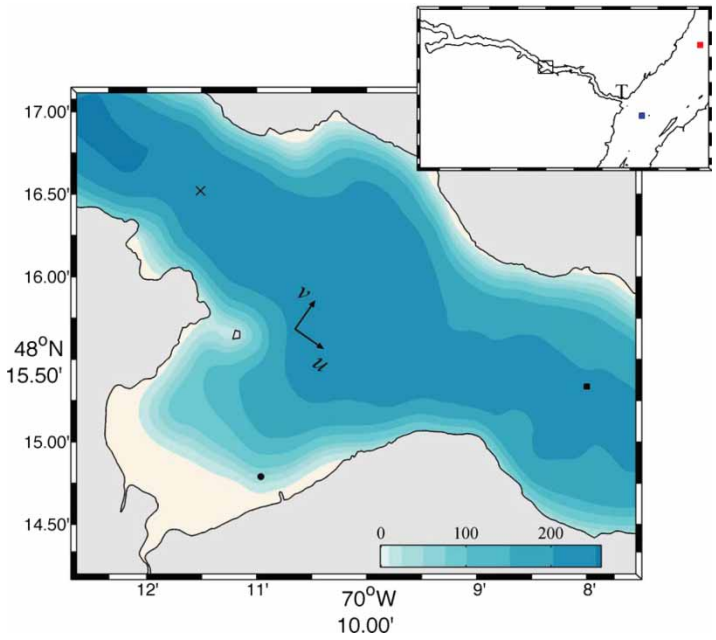

Fig. 2 Bathymetric chart of the sampling region site in Anse Saint-Jean in the Saguenay Fjord. The origin of the coordinate system is the location of the main sampling camp at 245 m depth. The solid black circle indicates the location of the main ice fishing area where equipment testing was done. The solid black square indicates the location where a CTD profile was collected at the end of the previous summer, on 22 September 2009, from the R/V *Coriolis II*. The solid red and blue squares in the St. Lawrence Estuary (inset) are the stations for which the temperature-salinity properties are presented in Fig. 13. The cross symbol is the station where historical ice thickness and snow depth measurements were collected by the Canadian Ice Service (see middle panel in Fig. 1).

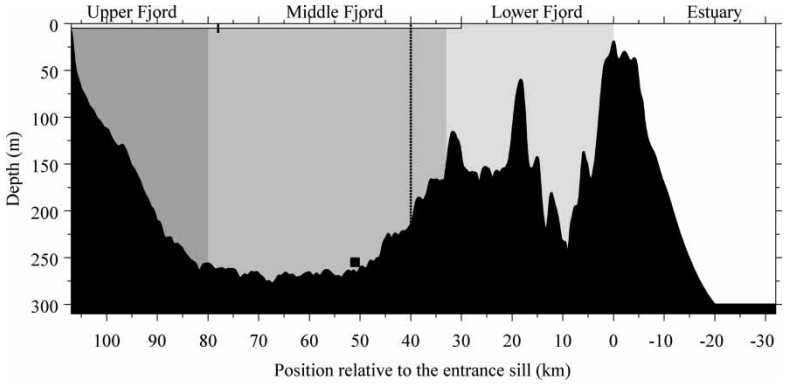

Fig. 3 Maximum cross-section depth along the length of the fjord and seaward into the St. Lawrence Estuary through the Laurentian Channel. The vertical shades of grey highlight the three geomorphological sections of the fjord (Locat and Lévesque, 2009). The thin horizontal rectangle near the surface indicates the ice coverage in February 2010. The dashed line represents the approximate location where measurements were collected for this study. The short solid line near the surface at kilometre 78 represents the depth interval over which measurements were collected in the winter of 1985–86 by Chassé and Côté (1991) and the square near the bottom at kilometre 50 represents the conductivity-temperature mooring deployed by Bélanger (2003) during winter 1998–99.

b *Summer Conditions*

Approximately 90% of the total volume of freshwater entering the fjord is injected at its head through the Saguenay River at an annual mean rate of 1200 (1100 and 1400) $m^3\ s^{-1}$, where the numbers in parentheses represent the winter minimum and spring maximum climatological values, respectively (Table 9 in Bélanger, 2003). The discharge of the Saguenay River has been regulated since 1926 at the Isle Maligne hydroelectric powerhouse, currently operated by Rio Tinto Alcan. The time series of the Saguenay River discharge rate for 2009–10 is shown in Fig. 4.

At the other extreme (kilometre 0 in Fig. 3), the fjord connects with the St. Lawrence Estuary where it discharges brackish surface water and receives approximately $10^7 m^3$ per tide of cold intermediate water that is pushed above sill crest every flood tide (Seibert et al., 1979). Whether this dense water can flow upfjord and across the second and third sills to renew the deep water of the Middle Fjord during summer is

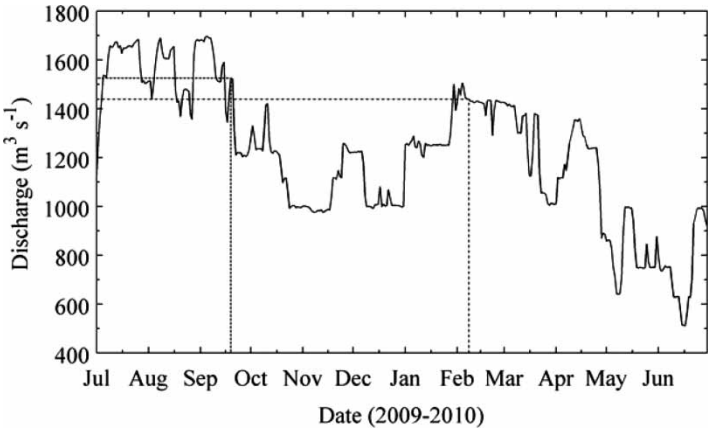

Fig. 4 Freshwater discharge rates of the Saguenay River for 2009/10. The dashed and dashed-dotted lines are visual aids located three days before the measurements presented in Fig. 8 were collected. Data were provided by Rio Tinto Alcan (M. Cormier, personal communication, 2011).

still not clear. This aspect of deep water renewal is reviewed in greater detail in Section 2c and will also be discussed in the light of our new observations and analysis (Section 5).

The summer water column of the Lower Fjord exhibits a two-layer salinity and temperature structure with a warmer ($T \simeq 10$°C) and fresher ($S \simeq 10$, practical salinity scale) top layer of thickness (varying between 5 and 20 m) overlying a cold ($T \simeq 2$°C) and salty ($S \simeq 30$) bottom layer (Fig. 5) (Drainville, 1968; Sundby and Loring, 1978; Schafer et al., 1990; Stacey and Gratton, 2001; Bélanger, 2003).

While the salinity structure of the Middle and Upper Fjord is similar to that of the Lower Fjord (Fig. 5), the temperature structure may show up to four distinct water masses (Fig. 5). Particularly intriguing in Drainville's (1968) observations is the

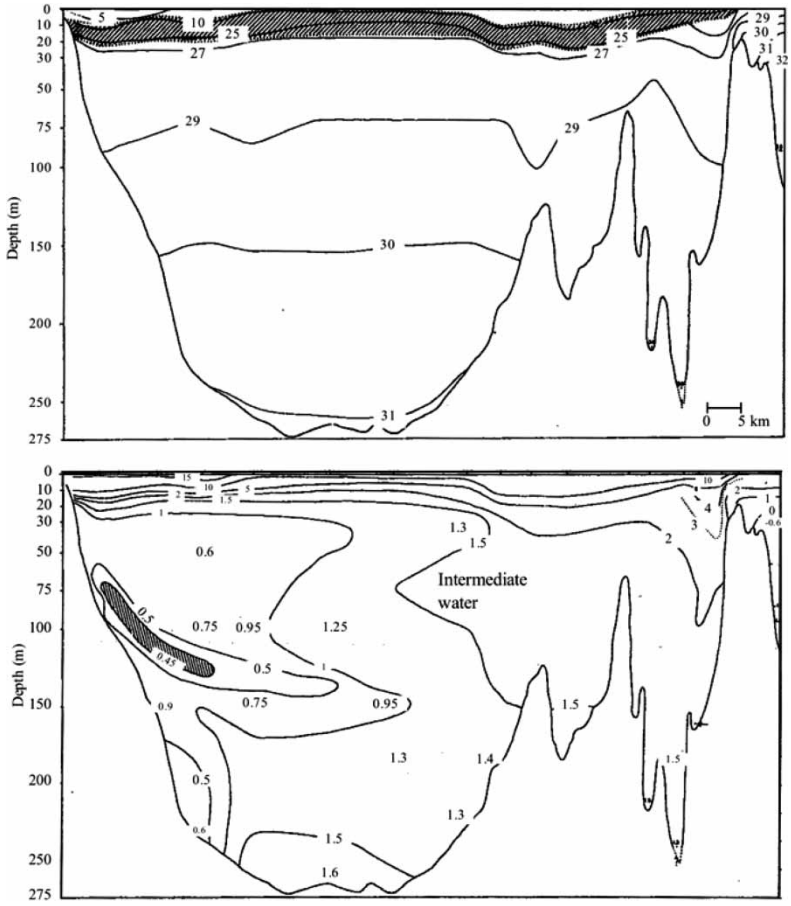

Fig. 5 Salinity (top panel) and temperature (°C; bottom panel) fields in June 1962 (adapted from Drainville, 1968 copied under licence from Copibec).

presence of an intermediate layer characterized by $T \simeq 1.5$°C and centred around 75 m depth (Fig. 5). The isotherm pattern suggests that this water is produced in the Lower Fjord and spreads up-fjord at intermediate depths. Similar intermediate water masses are also seen in the observations reported by Sundby and Loring (1978) for September 1974 and by Seibert et al. (1979) for July 1961 and August 1963. Although not as clear, the temperature field reported by Schafer et al. (1990) for November 1967 also shows indications of such an intermediate layer spreading into the Middle Fjord (their Fig. 4). While Drainville (1968) did not propose a mechanism for the origin of this water mass, Sundby and Loring (1978) suggested that it was produced by a partial renewal of the Middle Fjord that took place between May and September.

During summer, the coldest fjord waters characterized by $T \simeq 0.45$°C are found at mid-depth in the Upper Fjord (Fig. 5). Drainville (1968) suggested that this water mass was a remnant of cold water introduced into the Middle Fjord by deep water renewals during the previous winter (discussed below in greater detail). Finally, the saltiest water mass fills the bottom of the inner basin.

The fjord is dynamically "narrow" because the internal Rossby radius of deformation $R_i = \sqrt{g' h_1}/f \sim 10$ km, where g' is the reduced gravity, h_1 the thickness of the surface layer and f the Coriolis parameter, is greater than the typical fjord width (Cottier et al., 2010). For most applications, the fjord hydrography and circulation can therefore be approximated as being two-dimensionnal (e.g., Stacey and Gratton, 2001) although some cross-channel asymmetries in suspended sediment observed near the head have been attributed to the Coriolis force by Schafer et al. (1990).

According to numerical simulations and some observations (Stacey and Gratton, 2001; Bélanger, 2003), the top 50 m or so of the water column is characterized by a two-layer estuarine circulation with the top layer (0–20 m) flowing seaward and the underlying intermediate layer (20–50 m) flowing landward. At greater depth (>50 m) the circulation is more complex. For example, Stacey and Gratton (2001) suggested the existence of a bottom seaward flowing layer across the 60 m sill. They attributed this circulation to an up-fjord baroclinic pressure gradient across the sill caused by higher turbulent mixing rates on the seaward side of the sill. Similar three-layer circulations across sills are also seen in Bélanger's (2003) simulations.

The summer residual circulation is modulated by the tide that can reach amplitudes close to 3 m at the mouth with current speeds of approximately 0.5 m s^{-1} (Stacey and Gratton, 2001). The tides are mostly dissipated in the Lower Fjord and tidal currents are significantly weaker (<0.1 m s^{-1}) in the Middle and Upper Fjords (Schafer et al., 1990; Stacey and Gratton, 2001).

c *Winter Conditions*

The winter oceanographic conditions of the fjord are poorly documented. As mentioned in Section 1, there are no historical winter temperature-salinity (*T-S*) profiles published in the literature or available in public databases. Prior to the current work, our view of the *T-S* winter structure mostly relied on Drainville's (1968) hypotheses which suggested that winter atmospheric cooling and brine rejection caused by sea-ice formation generate sufficient deep convection to homogenize the temperature and salinity structures vertically. Drainville (1968) also hypothesized that such winter convection could be a significant source of deep water in the Middle Fjord. Drainville (1968) considered this deep water renewal mechanism plausible as long as the salinity of the surface water could be raised from about $S \approx 10$ in summer to $S \approx 26$ during winter. While quite large, Drainville (1968) considered this increase in surface salinity from summer to winter possible based on similar variations observed in a comparable subarctic fjord (Bute Inlet, British Columbia).

Only two studies have reported winter measurements. Chassé and Côté (1991) carried out a field experiment in the winter of 1985/86 at a site in the Middle Fjord (Fig. 2) to examine winter primary production in the surface layer (0–10 m). Their study provided bi-weekly, 10-month long, time series of temperature, salinity, nutrients, chlorophyll *a*, microalgal cells and primary production. Their observations show low surface salinity in winter, with $S \approx 3$ in February, and a stronger salinity difference between the surface and 10 m depth during winter than during summer, with $\Delta S \approx 16$ in February compared with $\Delta S \approx 1$ in the previous August. These observations do not support Drainville's (1968) hypotheses discussed above regarding the salinity conditions required to allow for local deep water formation. However, this aspect was not mentioned by Chassé and Côté (1991) but will be further discussed in the light of our new observations (Section 5).

The second source of winter measurements comes from Bélanger (2003) who moored a temperature-salinity sensor at the bottom of the Middle Fjord (Fig. 2) from June 1998 to March 1999 to document deep water renewal events. While Drainville (1968) raised the hypothesis that local winter convection may be a source of deep water, as discussed above, he also hypothesized that the deep water of the Middle Fjord may also come from cold water originating when the St. Lawrence Estuary spills over sills into the fjord. Drainville (1968) proposed that this mechanism of deep water renewal would be most effective during winter when water from the St. Lawrence Estuary would be cold enough, and thus sufficiently dense, to flow over sills and penetrate the Middle Fjord. This hypothesis was indirectly supported by Therriault and Lacroix (1975) who concluded that summer renewal events were not sufficiently intense to explain the characteristics of the deep water mass. They proposed that most of the renewals should occur in winter. This is supported by Bélanger (2003) who observed approximately 12 distinct deep water renewal events of which approximately four occurred during summer and the rest during fall and winter. Bélanger (2003) hypothesized that northeast winds over the St. Lawrence Estuary would be unfavorable to summer deep water renewal because they tend to pile-up light water at the mouth of the fjord, and that summer renewals occur primarily after long periods (on the order of weeks) without such winds.

On the other hand, Bélanger (2003) suggested that winter renewal events were linked primarily with the neap-spring tidal cycle with wind playing a secondary role.

3 Methods

An ice camp was set up on the ice of the Middle Fjord at the outer limit of Anse Saint-Jean where the water depth is 245 m (Figs 2 and 3). This area is the closest to the fjord's mouth that ice camps can be safely settled. Because of high tidal currents, the ice in the Lower Fjord, if any, is unstable. Measurements were collected from 2000 UTC, 10 February 2010 to 1300 UTC, 12 February 2010, a period corresponding to the transition from neap to spring tides.

A downward-looking 120 kHz Simrad echo-sounder was deployed on a fixed pod at 48°15.654′N and 70°10.644′W with the transducer located 0.6 m below the ice-water interface. The pulse duration was set to 256 μs and the sample interval to 4.8 cm. The echo-sounder sampled almost continuously from 2005 UTC, 10 February 2010 to 1315 UTC, 12 February 2010, except for a period of about five hours during the night of 10 February because of a power failure. The echo-sounder was post-calibrated for biomass detection on 6 May 2010 using facilities at the Institut Maritime du Québec, Rimouski.

A downward-looking 300 kHz Teledyne RD Instruments Workhorse acoustic Doppler current profiler (ADCP) was deployed on a fixed pod 0.8 m below the ice-water interface at 48°15.696′N and 70°10.697′W, roughly 50 m from the echo-sounder. The ADCP pinging and record rates were 1 Hz; the vertical bin size was 1 m; and the nominal range was 100 m. The ADCP sampled continuously for approximately the same period as the echo-sounder except for about one hour on 11 February while the data were downloaded. To reduce random noise, a 10-minute running mean filter was applied to the raw measurements. The uncertainty of the reduced velocity measurements is ±0.08 m s^{-1}. Currents were recorded in north-south, east-west coordinates. However, to facilitate the interpretation, the horizontal current vectors were rotated by 35° clockwise to produce along-channel (u) and across-channel (v) currents (see coordinate system in Fig. 2).

Fine-scale (approximately 10 cm) and micro-scale (approximately 1 cm) in situ water column measurements were obtained with a free-fall, loosely-tethered, coastal vertical microstructure profiler (VMP) manufactured by Rockland Scientific International (RSI). The VMP was equipped with two RSI SPM-38-1 airfoil shear probes (512 Hz sampling rate), a Sea-Bird Electronics, Inc. SBE-3F temperature sensor and an unpumped SBE-4C conductivity sensor (64 Hz sampling rate for the Sea-Bird sensors). The VMP was deployed at a distance of roughly 40 m from the echo-sounder and the ADCP (48°15.684′N and 70°10.650′W). Fifteen VMP profiles were collected between 1500 and 2200 UTC on 11 February. Fine-scale temperature and salinity measurements were reduced to a 1 m vertical bin size. The micro-scale shear measurements were used to calculate 4 m scale dissipation rates of turbulent kinetic energy ε (in W kg^{-1}) as in Bourgault et al. (2008) and Bourgault et al. (2011). Following Osborn (1980), the vertical eddy diffusivity was estimated as

$$K = \Gamma \frac{\varepsilon}{N^2}, \tag{1}$$

where $\Gamma = 0.2$ is taken as an upper bound flux coefficient and N is the 4 m scale buoyancy frequency defined as

$$N = \sqrt{-\frac{g}{\rho}\frac{\partial \rho}{\partial z}}, \tag{2}$$

where $g = 9.81$ m s^{-2} is the gravitational acceleration, z is the vertical axis (positive upward) and ρ is the re-ordered, gravitationally stable, density profile.

4 Observations

a *Ice*

The Upper and Middle Fjords were entirely ice-covered during the sampling period, except for a roughly 20 m wide channel that was opened by a Coast Guard icebreaker for the passage of commercial ships (Fig. 6). At the other end, the Lower Fjord was almost entirely ice free.

Although sampling was carried out during a year of record low ice coverage for the Gulf of St. Lawrence (see Fig. 1), it is not unusual for the Lower Fjord to be almost entirely ice free, even in years with anomalously high ice coverage in the Gulf, as in 2003 (Fig. 6). The Lower Fjord can thus be considered a polynya, likely caused by a combination of tidal mechanical energy that prevents ice consolidation, carrying it away from the area (latent heat polynya) and upwelling of warm water at sills that prevents ice formation (sensible heat polynya).

Ice throughout the bay was uniformly 50 cm thick and its surface was characterized by alternating patches of bare ice and thin (<5 cm) snow cover. Again, as noted above for the ice coverage, even though winter 2010 set a record low for ice conditions in the Gulf of St. Lawrence, the ice thickness was close to normal or perhaps even thicker than normal in the Saguenay Fjord, at least compared to the 1982–2001 period for which measurements exist (Fig. 1, middle panel). According to those measurements, the maximum ice thickness and standard deviation in Anse Saint-Jean is $h_{max} = 43 \pm 13$ cm. Snow cover was, however, much thinner than the 1982–2001 average (Fig. 1, middle panel).

Note that in 2002 Environment Canada stopped taking ice thickness and snow depth measurements in the Saguenay Fjord as well as in most subarctic regions (EC, 2011a). To complement the missing ice measurements, the duration of the ice fishing season can be used as a proxy for ice conditions in the Saguenay Fjord. This information is available in DFO (2011a). The fishing season starts when ice thickness reaches 30.5 cm and stops at a date fixed by the Canadian Coast Guard for icebreaking operations intended to prevent ice jams and flooding that can result from spring thaws. Since 1996 these operations have been carried out between 8 and 19 March of each year, except in 2010 when icebreaking

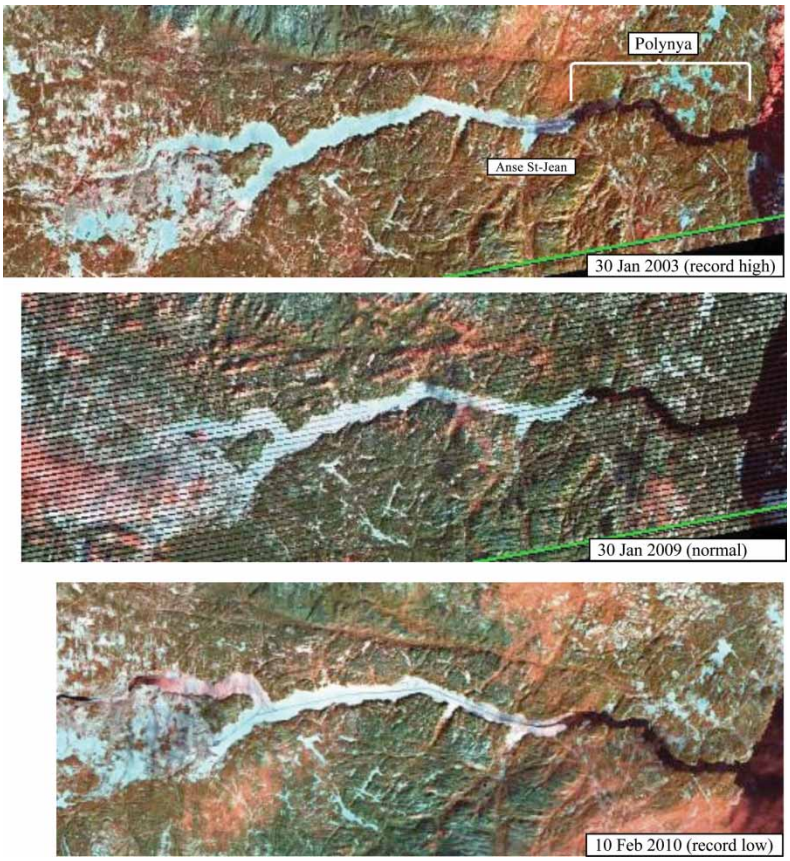

Fig. 6 Landsat satellite images comparing sea-ice cover in the Saguenay Fjord in the heart of winter for years with a record high (2003), normal (2009) and record low (2010) cover (see Fig. 1). Adapted from images retrieved online from the U.S. Geological Survey (USGS, 2011).

operations were exceptionally carried out on 19 February. The duration of the ice fishing season in winter 2010 reached a record low of 30 days compared with the 1996–2010 average and standard deviation of 60 ± 12 days (Fig. 1, bottom panel). The trend over this period is slightly negative with an average decrease of 0.4 days in the number of fishing days per year.

b *Currents and Water Properties*

The instantaneous horizontal currents exhibited fairly complex patterns characterized with episodic (<1 h), small-scale (<5 m vertical scale) and large variations (± 0.1 m s^{-1}) in temporal and vertical flow structures (Fig. 7). Although the flow was predominantly oriented along-channel (u), across-channel (v) effects are also important. The presence of the large bay and the island to the west (Fig. 2) likely induce complex across-channel effects in this area. The most striking and largest scale feature from those measurements is the semidiurnal variability that can be seen as alternating large patches of red and blue, especially in the along-channel component u. This semidiurnal variability is also clearly seen in the depth-averaged currents ($\bar{u}$, $\bar{v}$, Fig. 7, top panel). This variability is likely caused by the sum of M_2, S_2 and N_2 tidal constituents that provide the major semidiurnal tidal forcing at the mouth (Stacey and Gratton, 2001 their Table 1). The tidal currents are also presumably affected, but to a lesser extent, by a diurnal tidal variability induced by components such as K_1, O_1 or P_1 (Stacey and Gratton, 2001), but such a diurnal variability is hardly noticeable in the present data that span only 40 hours. Since the time series is too short to perform a harmonic analysis to discriminate between these components, a sinusoidal**,** least-squares fit to the deviation from the temporal mean of the depth-averaged currents was carried out instead to determine the period T and amplitudes ($\bar{u}_0$, $\bar{v}_0$) of the tidal signal observed. This analysis provided $T = 12.5$ h (i.e., close to the M_2 period) with $\bar{u}_0 = 0.07$ m s^{-1} and $\bar{v}_0 = 0.02$ m s^{-1}.

Over the water depth sampled (4–75 m) and sampling period (i.e., three semidiurnal tidal cycles and therefore about 1.5 diurnal cycles), the mean along-channel circulation exhibited more or less a three-layer structure (Fig. 8). The surface layer (4–11 m) was characterized by a strong, relative to tidal currents, seaward flow of maximum recorded velocity $U_{max} = 0.25$ m s^{-1} at 4 m depth. Note that the 0–4 m layer, not sampled with our ADCP setup, was likely characterized by a greater mean current, possibly up to $U_{max} = 0.5$ m s^{-1}, as suggested by visually extrapolating the measurements to the surface. Underneath (11–40 m), was a much weaker return flow of minimum velocity $U_{min} = -0.02$ m s^{-1}. Finally, below about 40 m was a thick seaward-flowing layer with $U_{max} = 0.03$ m s^{-1}.

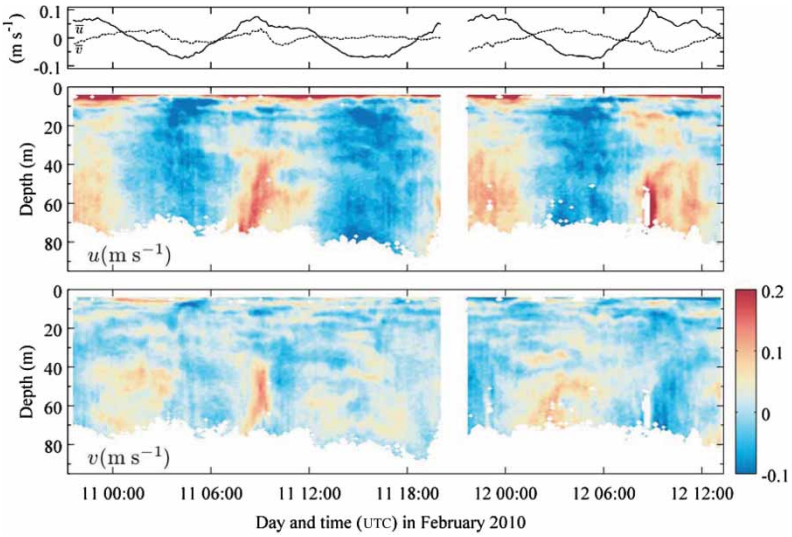

Fig. 7 Time series of the horizontal currents measured with the 300 kHz ADCP (10 min averages). (top panel) Along-channel ($\bar{u}$) and across-channel ($\bar{v}$) depth-averaged currents (i.e., within the depth interval 4–75 m). (middle panel) Time-depth distribution of the along-channel (u) and (bottom panel) across-channel (v) currents (1 m vertical bin size).

The temperature structure was characterized by three layers: a thin and very cold surface layer (0–5 m) of minimum temperature $T = -0.34$°C (i.e., close to the freezing point of seawater ($T_f = -0.39$°C for $S = 7.2$)); a warm intermediate layer (5–60 m) with a maximum temperature $T = 1.96$°C; and a thick (>60 m) bottom layer with a temperature $T = 0.66$°C (Fig. 8). The salinity structure was characterized by two layers separated by a sharp halocline located at 5 m depth. The surface layer (0–5 m) of minimum salinity $S = 7.2$ overlay a bottom layer (>5 m) of maximum salinity $S = 30.3$ near the bottom (Fig. 8). Both T and S showed little variation over the 7-hour sampling period (see the superimposed grey profiles in Fig. 8) even though these observations were collected during the transition between flood and ebb tides (see period between 1500 and 2200 UTC, 11 February in Fig. 7).

In comparison to conditions observed at the end of the previous summer at a nearby station, the temperature was about 10°C colder in the surface layer and about 2°C colder in the

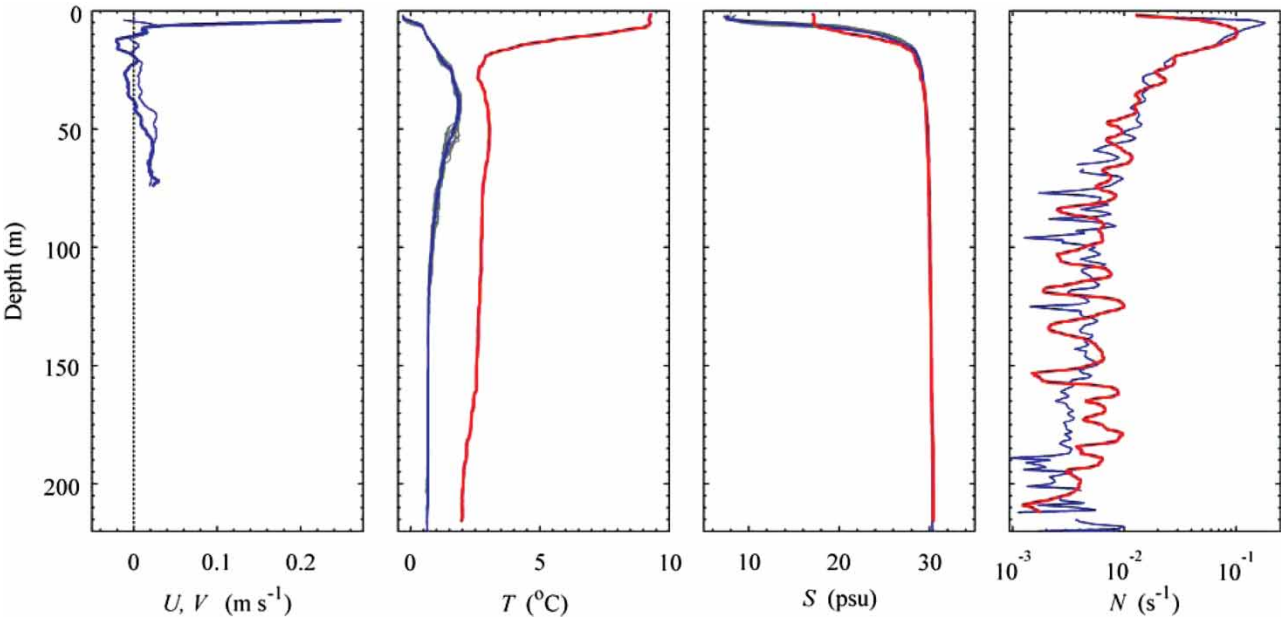

Fig. 8 Winter (blue curves) and summer (red curves) hydrographic conditions in Anse Saint-Jean. (first panel) Along-channel (thick) and across-channel (thin) mean circulation (U,V) computed by averaging the measurements presented in Fig. 7 over three semidiurnal tidal cycles. (last three panels) Temperature (T), salinity (S) and buoyancy frequency (N) profiles (1 m scale) observed 11 February 2010 between 1500 and 2200 UTC (the superimposed grey curves with their mean in blue; see Fig. 9 for exact timing) and at the end of the previous summer 22 September 2009 at a nearby station (red curves; see square on Fig. 2 for the exact location).

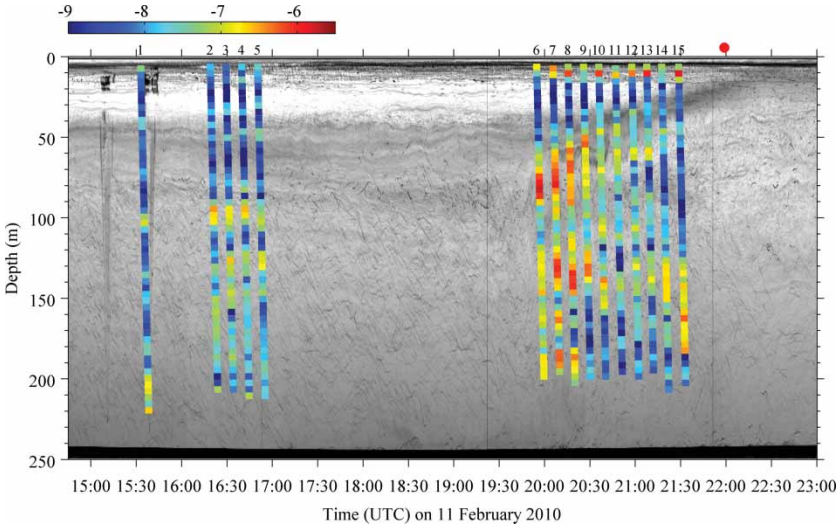

Fig. 9 Echogram at 120 kHz (grey scale, arbitrary units) and logarithm of the 4 m scale dissipation rate of turbulent kinetic energy relative to 1 W kg^{-1} (colour scale). VMP profiles are numbered from 1 to 15 at top of the figure. The solid red circle indicates time of sunset.

intermediate and bottom layers (Fig. 8). For salinity, the surface layer was about 10 fresher and 4 m thinner during winter with no significant difference between seasons in the salinity of the bottom layer. The winter pycnocline, characterized by the maximum buoyancy frequency $N_{max} = 0.16$ s^{-1} (i.e., period $\tau_{max} = 2\pi/N_{max} = 39$ s), was 60% stronger than at the end of the previous summer (Fig. 8).

c *Turbulence*

Dissipation rates of turbulent kinetic energy ε were patchy, changing by orders of magnitude over depths of mere metres (Fig. 9). Averaging all profiles depicts roughly three layers (Fig. 10): a surface layer (<15 m) with high dissipation rates and moderately high diffusivity ($\varepsilon \simeq 2 \times 10^{-7}$ W kg^{-1}, $K \simeq 7 \times 10^{-6}$m^2 s^{-1}); an intermediate layer (15–60 m) with low dissipation rates and low diffusivity ($\varepsilon \simeq 3 \times 10^{-9}$W kg^{-1}, $K \simeq 1 \times 10^{-6}$ m^2 s^{-1}); and a deep layer (>60 m) with moderately high dissipation rates and highest diffusivity ($\varepsilon \sim 10^{-7}$ W kg^{-1}, $K \sim 10^{-3}$m^2 s^{-1}).

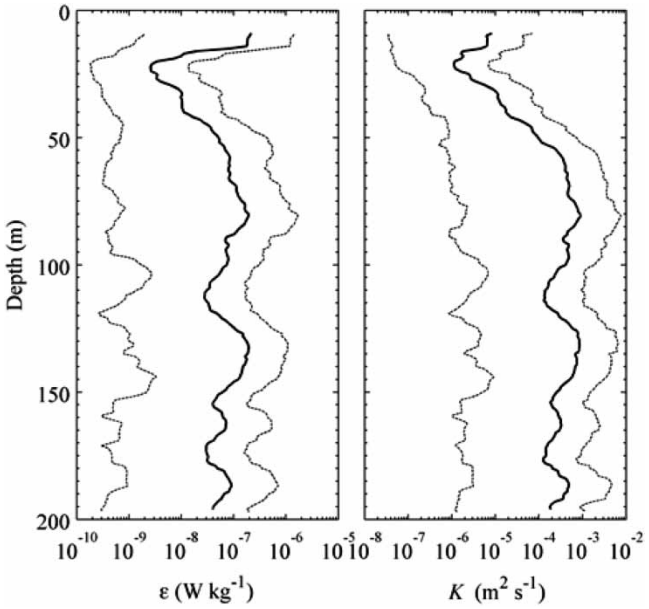

Fig. 10 Mean (solid line) and range (dashed lines) of dissipation rate of turbulent kinetic energy ε and eddy diffusivity K. Statistics computed from the 15 profiles collected (see Fig. 9 for individual ε profiles).

The time mean shear squared around the pycnocline, defined as

$$\overline{S^2_{pyc}} = \overline{\left(\frac{\partial u}{\partial z}\right)^2_{pyc}} + \overline{\left(\frac{\partial v}{\partial z}\right)^2_{pyc}}, \quad (3)$$

was $\overline{S^2_{pyc}} = 0.015$ s^{-2} with a maximum value reaching $\max(S^2_{pyc}) = 0.052$ s^{-2}. Relative to the buoyancy frequency squared at the pycnocline $N^2_{pyc} = 0.048$ s^{-2}, the shear suggests a dynamically stable pycnocline since the average Richardson number

$$\overline{\mathrm{Ri}}_{pyc} = \frac{N^2_{pyc}}{\overline{S^2_{pyc}}} = 3, \quad (4)$$

and the minimum

$$\min(\mathrm{Ri}_{pyc}) = \frac{N^2_{pyc}}{\max(S^2_{pyc})} = 1, \quad (5)$$

that is, with both cases being above the 1/4 threshold for instability (Miles, 1961).

d *Acoustic Properties*

Since in situ biological sampling was not carried out during this exploratory experiment, information on fish and zooplankton relies solely on acoustic properties at 120 kHz. Two quantities are used here to represent the acoustic

measurements: the volume backscattering strength S_v and the point backscattering strength S_p. Both quantities look qualitatively similar but they serve different purposes for quantitative assessments. The volume backscattering strength S_v is generally used for estimating zooplankton or fish abundance within a sample volume and the point backscattering strength S_p is used to characterize individual fish or targets (e.g., Simmonds and MacLennan, 2005). Making quantitative assessments from echo-sounder measurements requires ground-truth biological observations for calibration. Such observations are not available such that the echo-sounder measurements are used mostly as a qualitative means for describing the acoustic properties of the water column.

The volume backscattering strength S_v depicts a series of distinct biological and physical layers throughout the water column (Fig. 11). These layers become more apparent in the vertical profile of the daytime average volume backscattering strength $\overline{S_v}$ (Fig. 11, right panel) that could be considered as the background acoustic field. The strongest daytime signal with $\overline{S_v} = -70(-98, -66)$ dB, where the numbers in parentheses represent the 95% spread of the data, is located at the pycnocline, possibly caused by the concentration of particles or organisms or as a result of the sharp density gradient. The weakest daytime signal, with $\overline{S_v} = -103(-108, -95)$ dB, is oberved at 25 m depth, suggesting little presence of organisms in that layer. Below 50 m, the signal shows little variation with depth with $\overline{S_v} = -89(-93, -81)$ dB (average between 50 and 100 m). At greater depths (> 125 m), instrumental noise becomes more apparent and increasingly obscures the signal.

These layers are also seen in the point backscattering strength field S_p (Fig. 12). The top 5 m or so of the water column (i.e., the surface layer of minimum salinity $S = 7.2$ (Fig. 8)) is characterized by weak echoes ($S_p = -110$ dB) suggesting little presence of organisms in that layer. The layer underneath, between 5 m and 20 m, is characterized by a series of oscillating horizontal layers with $-80 < S_p < -70$ dB. Near the pycnocline, the oscillations are characterized by amplitude $a = 0.5$ m and period $\tau = 40$ s, close to the buoyancy period at the pycnocline $\tau_{max} = 39$ s. These oscillations are likely small-amplitude high-frequency internal waves of unknown origin. Without in situ biological observations it cannot be determined unambiguously whether these layers reflect physical or biological properties. This 5–20 m stratum is also characterized by the presence of scattered targets, most probably small fish characterized by $S_p \approx -55$ dB.

The stratum underneath, between 20 m and 35 m, shows low echo intensities and no fish targets, except around the time of sunset (2200 UTC) when this layer becomes filled with presumably vertically migrating zooplankton. Prior to the migration, during daytime, this zooplankton concentration is visible as a cloudy layer with $S_v \approx -85$ dB approximately located between 35 m and 80 m (i.e., approximately between 1430 and 2030 in Fig. 11). The upward migration starts between 2030 UTC and 2100 UTC and is completed by 2215 UTC during which time the zooplankton have covered a distance of about 50 m. The vertical swim speed can therefore be estimated as $w_{zoo} = 50$ m/5400 s ≈ 1 cm s^{-1}, consistent with copepods and euphausids (Vlymen, 1970; Wiebe et al., 1992). We observed an increase in the values of S_v to about −75 dB during the suggested migration event. A number of factors may be responsible for such an increase, such as an increase in concentration of mesozooplankton, an increase in the average size of individuals and/or a swarming event of less abundant species such as euphausiids or hyperriid amphipods (Cottier et al., 2006).

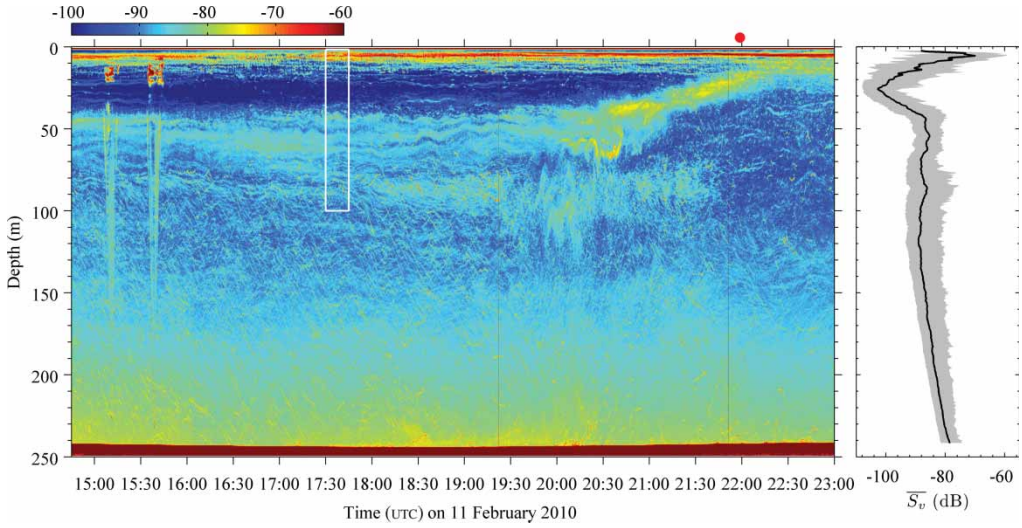

Fig. 11 (left panel) Volume backscattering strength S_v (dB re 1 m^{-1}) at 120 kHz and (right panel) daytime average profile $\overline{S_v}$ (black solid line) and 95% spread of the data (grey shade). The daytime average is taken between 1545 and 1600 UTC. The solid red circle indicates the time of sunset. The point backscatter strength S_p within the white box is shown in greater detail in Fig. 12. The two v-like traces between 1500 and 1545 UTC are interference caused by the VMP that was initially deployed too close to the transducer. Those instruments were moved about 40 m away from the transducer for subsequent profiles.

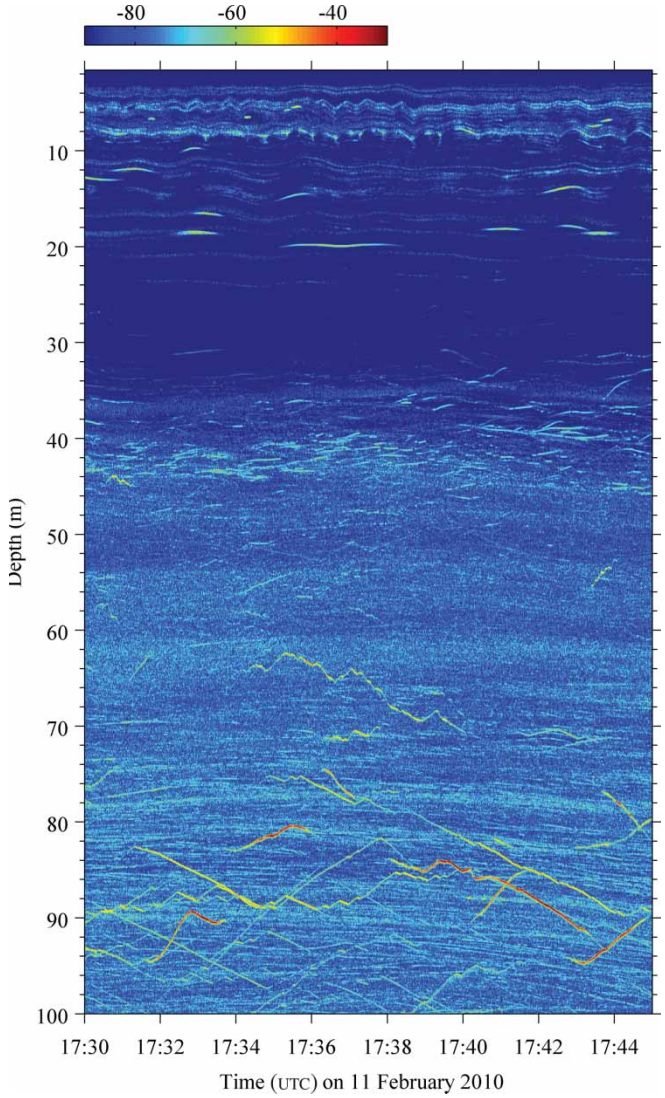

Fig. 12 Point backscattering strength S_p (dB re 1 m^{-2}) (dB) at 120 kHz (details of white box in Fig. 11).

Summer mesozooplankton in the Middle Fjord is characterized mostly by small copepod species such as *Microcalanus, Oncaea* and *Oithona* compared to the zooplankton composition at the head of the Saguenay Fjord, where large copepods such as *Calanus* dominate (DeLadurantaye et al., 1984). As we do not have any biological data, we are unable to determine which factor may be of importance to our study.

Finally, the bottom layer of the echogram, starting from the base of the zooplankton layer, around 80 m, and extending down to the bottom, is filled throughout the day and night with oblique traces of varying echo intensities. In this space-time representation, these traces indicate fish movements with vertical excursions of 10–20 m in 4–5 min. This contrasts with the fish targets observed in the 5–20 m layer that appear more passive. The highest intensities reach about $S_p \approx -35$ dB, suggestive of large adult fish found in the fjord (DFO, 2008, 2011a).

5 Discussion

a *Drainville's Hypotheses*

As mentioned in Section 2, Drainville (1968) proposed some hypotheses regarding the winter oceanographic conditions of the fjord. One of these hypotheses was that during winter the temperature becomes vertically homogeneous and the halocline diminishes, perhaps even disappears. That hypothesis is refuted by this field experiment, at least for the ice-covered Middle Fjord. The temperature structure observed in winter 2010 in the Middle Fjord was stratified into three layers: a very cold surface layer (T close to freezing), a warm intermediate layer ($T \simeq 2$°C) and a cold bottom layer ($T \simeq 0.7$°C). The halocline was also stronger during winter 2010 than it was during summer 2009.

Could the stronger halocline and fresher surface salinity in winter 2010 relative to the previous summer be attributed to a greater freshwater discharge rate of the regulated Saguenay

River? Given the mean surface layer current of roughly 0.3 m s^{-1} (Fig. 8) it takes about three days for a change in the freshwater discharge rate of the Saguenay River, approximately 60 km landward, to appear at the sampling site in Anse Saint-Jean. Taking this three-day lag into consideration the discharge rate measurements (Fig. 4) suggest that the amounts of freshwater in Anse Saint-Jean were comparable in the two seasons, with in fact about 5% less freshwater during the winter sampling. The mean hydrological conditions were, thus, similar during the two seasons and cannot explain the stratification difference.

However, we note that although the summer halocline was weaker, the surface layer was thicker. It would therefore be meaningful to compare the freshwater content h, in metres, for the two seasons. This is defined as

$$h = \int_{z_0}^{0} \frac{S_0 - S}{S_0} dz, \tag{6}$$

where $S_0 = 29.5 \pm 0.5$ is the reference salinity chosen as representative of the base of the surface layer and z_0 is the depth at which $S = S_0$. The calculation shows that the freshwater content between the two seasons are comparable with $h_{\mathrm{Feb}} = 4.8 \pm 0.4$ m for winter and $h_{\mathrm{Sep}} = 5.2 \pm 0.5$ m for summer. The 8% higher freshwater content in September 2009, compared to February 2010, may be attributed to a correspondingly similar higher discharge rate of the Saguenay River (Fig. 4). Given that both sampling periods were subject to similar hydrological forcing and had comparable freshwater content, the other possibility to explain the stronger winter halocline and thinner surface layer is the sea-ice shielding effect on wind-induced mixing.

Drainville (1968) also hypothesized that a fraction of the deep water in the Middle Fjord may originate from local deep winter convection. Our observations do not support this hypothesis. We did not observe a winter mixed layer reaching the bottom but rather a 4 m thick surface mixed layer separated by a strong and dynamically stable halocline that minimizes exchanges with the bottom water.

b *Origin of the Saguenay Intermediate Water (SIW) and Deep Water*

We have identified in our conductivity, temperature, depth (CTD) profiles a layer we described in Section 4 as being a warm intermediate layer. This layer was characterized in winter 2010 by a maximum temperature $T_{\max} \simeq 2$°C centred at about 40 m. Clues about the origin of this layer appear when comparing the February 2010 and September 2009 data on a *T-S* diagram (Fig. 13). The *T-S* diagram clearly reveals the existence of this layer during the previous summer with a similar salinity $S = 29.7$ but warmer temperature $T_{\max} \simeq 3$°C. This suggests that this intermediate water was not produced by winter processes but was produced during summer, by a mechanism to be discussed below, with subsequent erosion during winter.

As presented in Section 2, similar intermediate layers in the Middle Fjord are also seen in Drainville's (1968) observations (Fig. 5) as well as in Sundby and Loring (1978), Seibert et al. (1979) and Schafer et al. (1990). These repetitive occurrences suggest that this layer is a persistent feature of the Saguenay Fjord that appears as a warm intermediate layer during winter and simply as an intermediate layer during summer. We propose to name this water mass the Saguenay Intermediate Water (SIW).

All observations reported in the literature cited above suggest that the SIW originates in the Lower Fjord and spreads up-fjord at mid-depth into the Middle Fjord. The *T-S* diagram further suggests that SIW could be a mixture of cold intermediate layer (CIL) water, found during summer in the St. Lawrence Estuary and at the mouth of the fjord at flood tide, and Saguenay surface water. This is illustrated in Fig. 13 with the mixing line joining these water types. Every flood tide some CIL water is pushed against the sill at the Head of the Laurentian Channel and enters the Lower Fjord (Seibert et al., 1979). We hypothesize that intense mixing at sills, and more generally throughout the Lower Fjord where tidal currents are large, mixes CIL water with surface Saguenay water to produce SIW spreading up-fjord. This process can also be regarded as a mechanism

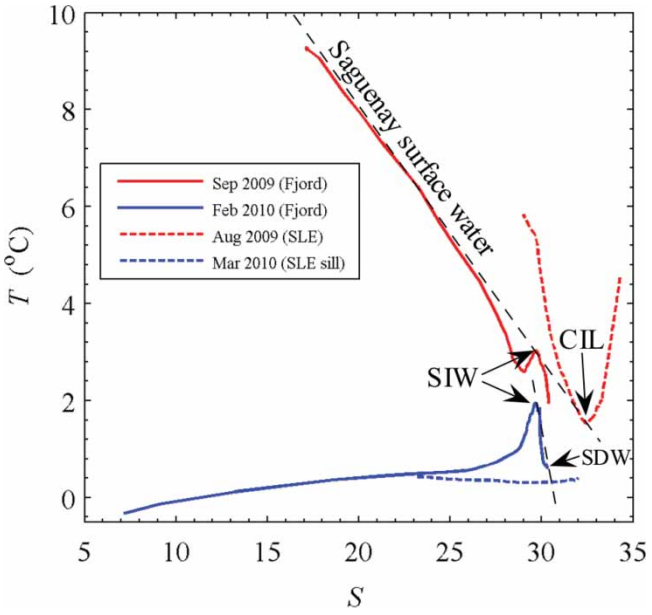

Fig. 13 *T-S* diagram. The solid red and blue curves represent, respectively, conditions in Anse Saint-Jean in winter 2010 (11 February) and summer 2009 (22 September). The red dashed curve represents conditions in the Lower St. Lawrence Estuary (red square on Fig. 2) in summer 2009 (29 August) and the dashed blue curve represents conditions at the mouth of the fjord (blue square on Fig. 2) in winter 2010 (9 March). CIL stands for the Cold Intermediate Layer of the St. Lawrence Estuary; SIW stands for Saguenay Intermediate Water and SDW for Saguenay Deep Water. The black dashed lines are visual aids to show, respectively, the mixing lines between the Saguenay surface water and the CIL producing SIW and between winter St. Lawrence Estuary water found at the mouth of the fjord and SIW producing SDW.

for partial renewal of the Middle Fjord, as suggested by Sundby and Loring (1978).

As discussed in the previous section, local winter production of deep water in the Middle Fjord appears unlikely. The deep winter water more likely originates from spilling over sills of cold and salty water from the St. Lawrence Estuary, a mechanism also hypothesized by Drainville (1968) and documented by Bélanger (2003). This is also supported by the *T-S* diagram (Fig. 13). The diagram shows that it is possible to form the Saguenay Deep Water by mixing water found in the St. Lawrence Estuary near the mouth of the fjord during winter with SIW. In fact, during winter the deep waters of the Saguenay are warmer than any of the waters found on the Estuary side of the sill (Fig. 13). The only source of heat that could form these waters is from the SIW. This suggests that during winter the intruding St. Lawrence Estuary water, of higher salinity (and density) than in summer, mixes with the remnant of the previous summer's SIW rather than with the lighter Saguenay surface water to form the deepest water found in the Middle Fjord. In this view, the formation of SIW during summer is required for the production of these deep waters in winter.

c *Biologically Generated Turbulence?*

Based on turbulence measurements collected in Saanich Inlet, Kunze et al. (2006) suggested that the vertical migration of highly concentrated layers of macrozooplankton may be an important mixing mechanism in coastal systems. This hypothesis of biologically generated turbulence has since been the subject of debate (Kunze et al., 2007; Visser, 2007a, 2007b) and no consensus has been reached on the role that zooplankton may play in coastal ocean mixing. More extensive observations analyzed by Rousseau et al. (2010) rather support that biologically induced mixing by migrating zooplankton may be a rare phenomenon.

Here, we coincidently measured turbulence during a vertical migration event. About three profiles were collected at the heart of the migration (profiles 13–15 in Fig. 9). Although there appears to be enhanced mixing rates near the beginning of the migration, there is no evidence of sustained enhanced turbulence during the event that can be unequivocally associated with zooplankton migration.

6 Summary and conclusions

In this paper we have presented what appears to be the first historical measurements throughout the entire water column of the winter oceanographic conditions in the Saguenay Fjord, situated within the limits of the unique Saguenay–St. Lawrence Marine Park. The observations reveal that, contrary to Drainville's (1968) hypotheses, the water column is well stratified both in temperature and salinity during winter. In fact, when compared to the previous summer the water column was found to be more stratified with a thinner and fresher surface layer lying above a sharper halocline. We have attributed this stronger winter stratification to the shielding effect of sea ice to wind-induced mixing.

We have also identified a water mass that we propose to name Saguenay Intermediate Water (SIW). This water mass clearly appeared in winter 2010 as a warm intermediate layer of maximum temperature $T_{max} = 2°C$ lying between 20 and 60 m depth. This water mass is also seen on a *T-S* diagram when examining the previous summer's data but characterized with warmer temperature around $T_{max} = 3°C$. We have hypothesized that this water mass is formed during summer as a mixture of St. Lawrence Estuary Cold Intermediate Layer (CIL), which spills over the entrance sill at flood tide, and Saguenay surface water.

Our observations also provide a wintertime echogram of the water column. Although qualitative, the echogram reveals a series of biological strata with the presence of small fish near the top of the water column (5–20 m), showing little movement, and active larger fish at greater depth, below 80 m. The echogram also shows vertical migration of zooplankton, possibly euphausiids, mysids or hyperiid amphipod at sunset.

Subarctic marine environments such as the Saguenay Fjord offer great opportunities to study outstanding oceanographic questions related to boreal ice-covered marine ecosystems. While research should certainly continue in the Canadian Arctic we wish to encourage the oceanographic community to consider carrying out intensive research in subarctic Canada as well. To our knowledge no winter-long surveys mobilizing a scientific icebreaker 24 hours a day, 7 days a week have ever been carried out in the ice-covered Canadian subarctic, such as the Gulf of St. Lawrence and its connected bays and fjords, while this has already been done more than once in the Canadian Arctic (e.g., Fortier et al., 2008; Barber et al., 2010). As mentioned in the Section 1, Canadian subarctic marine environments are subject to similar winter climatic variabilities and anthropogenic stresses (e.g., proposed oil and gas exploration) as the Canadian Arctic. Without proper monitoring and more detailed research about the current state of subarctic Canadian ice-covered seas it would be difficult to foresee their evolution or to make proper environmental assessments with potentially important impacts on society and the economy.

Acknowledgements

This research was funded by the Natural Sciences and Engineering Research Council of Canada, the Canada Foundation for Innovation, the Department of Fisheries and Oceans Canada and is a contribution to the scientific program of Québec-Océan. We wish to thank Sylvain Blondeau and Michel Gosselin for their participation to the field work.

References

BARBER, D.G.; M.G. ASPLIN, Y. GRATTON, J. LUKOVICH, R.J. GALLEY, R. L. RADDATZ and D. LEITCH. 2010. The International Polar Year (IPY) Circumpolar Flaw Lead (CFL) system study: Overview and the physical system. *Atmosphere-Ocean,* **48**(4): 225–243, doi:10.3137/OC317.2010

BÉLANGER, C. 2003. *Observation and modelling of a renewal event in the Saguenay Fjord*. Ph.D. thesis, Université du Québec à Rimouski, Rimouski, Québec.

BOURGAULT, D.; D.E. KELLEY and P.S. GALBRAITH. 2008. Turbulence and boluses on an internal beach. *J. Mar. Res.* **66** (5): 563–588.

BOURGAULT, D.; D.C. JANES and P.S. GALBRAITH. 2011. Observations of a large-amplitude internal wavetrain and its reflection off a steep slope. *J. Phys. Oceanogr.* **41**: 586–600, doi:10.1175/2010JPO4464.1

CHASSÉ, R. and R. CÔTÉ. 1991. Aspects of winter primary production in the upstream section of Saguenay Fjord. *Hydrobiologia,* **215**(3): 251–260.

COMISO, J.C.; C.L. PARKINSON, R. GERSTEN and L. STOCK. 2008. Accelerated decline in the Arctic sea ice cover. *Geophys. Res. Lett.* **35**: L01703, doi:10.1029/2007GL031972

COTTIER, F.R.; G.A. TARLING, A. WOLD and S. FALK-PETERSEN. 2006. Unsynchronized and synchronized vertical migration of zooplankton in a High Arctic fjord. *Limnol. Oceanogr.* **51** (6): 2586–2599.

COTTIER, F.R.; F. NILSEN, R. SKOGSETH, V. TVERBERG, J. SKAROHAMAR and H. SVENDSEN. 2010. Arctic fjords: a review of the oceanographic environment and dominant physical processes. *Gelogical Society, London, Special Publications,* **344**: 35–50, doi:10.1144/SP344.4

DELADURANTAYE, R.; J.-C. THERRIAULT, G. LACROIX and R. CÔTÉ. 1984. Processus advectifs et répartition du zooplancton dans un fjord. *Mar. Biol.* **82**: 21–29.

DFO (Department of Fisheries and Oceans). 2008. *The Saguenay Fjord winter sport fishery in 2007*. DFO Can. Sci. Advis. Sec. Advis. Rep. 2007/050.

DFO (Department of Fisheries and Oceans). 2011a. *The Saguenay Fjord winter recreational groundfish fishery, 2008–2010*. DFO Can. Sci. Advis. Sec. Advis. Rep. 2010/088.

DFO (Department of Fisheries and Oceans). 2011b. *ODMS-Oceanographic Data Management System* [Data]. Retrieved from the Maurice Lamontagne Institute website: http://slgo.ca/app-sydo/en/accueil.html

DRAINVILLE, G. 1968. Le fjord du Saguenay: I. Contribution à l'océanographie. *Naturaliste Can.* **95** (4): 809–855.

EC (Environment Canada). 2011a. *Ice thickness data* [Data]. Retrieved from the Canadian Ice Service website: http://www.ec.gc.ca/glaces-ice/default.asp?lang=En&n=EIB31290-1

EC (Environment Canada). 2011b. Canadian Ice service-Ice Graph 1.03. Retrieved from http://ice-glaces.ec.gc.ca/IceGraph103/

FORTIER, L.; D. BARBER and J. MICHAUD (Eds). 2008. *On thin ice: a synthesis of the Canadian Arctic Shelf Exchange Study (CASES)*. Winnipeg, MB, Canada: Aboriginal Issues Press.

HOLLAND, M.M.; M.C. SERREZE and J. STROEVE. 2008. The sea ice mass budget of the Arctic and its future change as simulated by coupled climate models. *Clim. Dyn.* **34**: 185–200, doi:10.1007/s00382-008-0493-4

JANES, D.C. 2009. *Sill processes in the Saguenay Fjord*. M.S. thesis, Physics and Physical Oceanography, Memorial University, St. John's, Newfoundland, Canada.

KUNZE, E.; J. DOWER, I. BEVERIDGE, R. DEWEY and K. BARTLETT. 2006. Observations of biologically generated turbulence in a coastal inlet. *Science,* **313**: 1768–1770.

KUNZE, E.; J. DOWER, R. DEWEY and E.A. D'ASARO. 2007. Mixing it up with krill. *Science,* **318**: 1239.

LOCAT, J. and C. LÉVESQUE. 2009. Le fjord du Saguenay: Une physiographie et un registre exceptionnels. *Revue des Sciences de l'Eau,* **22** (2): 135–157.

MILES, J. 1961. On the stability of heterogeneous shear flows. *J. Fluid Mech.* **10**: 496–508.

OSBORN, T.R. 1980. Estimates of the local rate of vertical diffusion from dissipation measurements. *J. Phys. Oceanogr.* **10**: 83–89.

PARKINSON, C.L. and D.J. CAVALIERI. 2008. Arctic sea ice variability and trends, 1979–2006. *J. Geophys. Res.* **113**: C07003, doi:10.1029/2007JC004558

PELLETIER, E. and J.-M. SÉVIGNY. 2009. *Parc marin Saguenay - Saint-Laurent. Dix années de recherche et de conservation*, E. Pelletier and J.-M. Sévigny, Eds., Revue des sciences de l'eau.

ROUSSEAU, S.; E. KUNZE, R. DEWEY, K. BARTLETT and J. DOWER. 2010. On the efficiency of turbulence production by swimming marine organisms in the open ocean and coastal waters. *J. Phys. Oceanogr.* **40**: 2107–2121, doi:10.1175/2010JPO4415.1

SCHAFER, C.T.; J.N. SMITH and R. CÔTÉ. 1990. The Saguenay Fiord: A major tributary to the St. Lawrence Estuary. In M.I. El-Sabh and N. Silverberg (Eds), *Oceanography of a large-scale estuarine system: The St. Lawrence.* (pp. 378–420). New York: Springer-Verlag.

SEIBERT, G.H.; R.W. TRITES and S.J. REID. 1979. Deepwater exchange processes in the Saguenay Fjord. *J. Fish. Res. Board Can.* **36**: 42–53.

SIMMONDS, J. and D. MACLENNAN. 2005. *Fisheries acoustics - Theory and practice,* 2nd Edition. Ames, Iowa: Blackwell Science Ltd.

STACEY, M.W. and Y. GRATTON. 2001. The energetics, and tidally induced reverse renewal in a two-silled fjord. *J. Phys. Oceanogr.* **31**: 1599–1615.

STROEVE, J.; M.M. HOLLAND, W. MEIER, T. SCAMBOS and M. SERREZE. 2007. Arctic sea ice decline: Faster than forecast. *Geophys. Res. Lett.* **34**: L09501, doi:10.1029/2007GL029703

SUNDBY, B. and D.H. LORING. 1978. Geochemistry of suspended particulate matter in the Saguenay Fjord. *Can. J. Earth Sci.* **15**: 1002–1011.

THERRIAULT, J.-C. and G. LACROIX. 1975. Penetration of the deep layer of the Saguenay Fjord by surface waters of the St. Lawrence Estuary. *J. Fish. Res. Board Can.* **32**: 2373–2377.

USGS (United States Geological Survey). 2011. USGS global visualization viewer. Retrieved from http://glovis.usgs.gov/

VISSER, A.W. 2007a. Biomixing of the oceans? *Science,* **316**: 838–839.

VISSER, A.W. 2007b. Mixing it up with krill. *Science,* **318**: 1239–1239.

VLYMEN, W.J. 1970. Energy expenditure of swimming copepods. *Limnol. Oceanogr.* **15**: 348–356.

WIEBE, P.H.; N.J. COPLEY and S.H. BOYD. 1992. Coarse-scale horizontal patchiness and vertical migration of zooplankton in Gulf Stream warm-core ring 82-H. *Deep-Sea Res.* **39** (suppl): S247–S278.